

Anisotropies of different mass compositions of cosmic rays

Bing-Qiang Qiao,^{a,b,1} Wei Liu,^{c,1} Yi-Qing Guo,^{c,1} Qiang Yuan^{a,b,d,1}

^aKey Laboratory of Dark Matter and Space Astronomy, Purple Mountain Observatory, Chinese Academy of Sciences, Nanjing 210008, China

^bSchool of Astronomy and Space Science, University of Science and Technology of China, Hefei 230026, China

^cKey Laboratory of Particle Astrophysics, Institute of High Energy Physics, Chinese Academy of Sciences, Beijing 100049, China

^dCenter for High Energy Physics, Peking University, Beijing 100871, China

E-mail: qiaobq@ihep.ac.cn, liuwei@ihep.ac.cn, guoyq@ihep.ac.cn, yuanq@pmo.ac.cn

Abstract. The spectral hardenings of cosmic ray nuclei above ~ 200 GV followed by softenings around 10 TV, the knee of the all-particle spectrum around PeV energies, as well as the pattern change of the amplitude and phase of the large-scale anisotropies around 100 TeV indicate the complexities of the origin and transportation of Galactic cosmic rays. It has been shown that nearby source(s) are most likely to be the cause of such spectral features of both the spectra and the anisotropies. In this work, we study the anisotropy features of different mass composition (or mass groups) of cosmic rays in this nearby source model. We show that even if the spectral features from the nearby source component is less distinctive compared with the background component from e.g., the population of distant sources, the anisotropy features are more remarkable to be identified. Measurements of the anisotropies of each mass composition (group) of cosmic rays by the space experiments such as DAMPE and HERD and the ground-based experiments such as LHAASO in the near future are expected to be able to critically test this scenario.

¹Corresponding author.

Contents

1	Introduction	1
2	Model Description	2
2.1	Spatially-dependent diffusion	2
2.2	Local source	3
2.3	Sun's vertical location	3
3	Results	3
4	Discussion	7

1 Introduction

It is widely postulated that cosmic rays (CRs) with energies less than \sim PeV are mainly generated by the Galactic supernova remnants (SNRs). Through the well-known diffusive shock acceleration process inside SNRs [1–4], CRs are accelerated to form non-thermal power-law spectra, $dN/d\mathcal{R} \propto \mathcal{R}^{-\nu}$, with \mathcal{R} being the rigidity. After escaping from the acceleration sites, they undergo frequent scatterings with the random magnetic turbulence in the Galaxy, whose behaviours are usually described by a diffusion equation. In the conventional propagation model, the diffusion is assumed to be homogeneous and isotropic, with a rigidity-dependence, namely $D(\mathcal{R}) \propto \mathcal{R}^{\delta}$, with δ being constrained from 0.3 to 0.6 from the Boron-to-Carbon ratio [5]. The propagated CR spectrum should then fall as $\phi \propto \mathcal{R}^{-\nu-\delta}$. Aside from the diffusion, CR nuclei may also suffer from the convection, re-acceleration as well as the fragmentation by collision with the interstellar gas. The low-energy nuclei also lose their energies due to the ionization and Coulomb scattering. For a comprehensive introduction to the CR propagation in the Galaxy, one can refer to [6, 7].

The convective CR transport picture has successfully reproduced the observed power-law spectrum, the secondary-to-primary ratio, e.g. B/C ratio, the diffuse gamma-ray distribution and so on. However, growing observations challenge the conventional transport model. In recent years, the hardening of CR spectra above a few hundred GeV/nucleon received much attention. They were initially observed by balloon-borne calorimeter experiments ATIC-2 [8, 9], CREAM [10, 11], and get confirmed by precise measurements of space magnetic spectrometer experiments PAMELA [12] and AMS-02 [13, 14] and calorimeter experiment CALET [15]. The finding of the spectral hardenings brings about various alternatives to the traditional CR paradigm (e.g. [16–21]). Most recently, the DAMPE observation shows clearly that the proton spectrum further experiences a spectral softening at ~ 14 TeV [22]. Hints of such spectral features were also found previously by CREAM [23] and NUCLEON measurements [24]. These new observations indicate that the structures of the energy spectra of CRs are more complicated than expected (see e.g., [25, 26] for discussions).

In addition to the unexpected structures in CR energy spectra, the traditional transport scenario also fails to explain the observed anisotropies. Despite that the arrival directions of Galactic CRs are highly isotropic due to their diffusive propagation in the Galactic magnetic field, a weak dipole-like anisotropy is consistently observed, with intensity differences up to $\sim 10^{-4} - 10^{-3}$. So far a large amount of observations of anisotropies ranging from TeV to PeV

have been carried out by the ground-based experiments, for example Super-Kamiokande [27], Tibet [28–31], Milagro [32, 33], IceCube/Ice-Top [34–38], ARGO-YBJ [39, 40] and HAWC [41]. Besides the large-scale anisotropies, some mediate-scale and small-scale anisotropies have also been measured [38, 41, 42].

One of the well-known origins of the large-scale anisotropy is the so-called Compton-Getting effect [43, 44], which is induced by the motion of solar system with respect to a frame in which CR distribution is isotropic. This effect only relies on the power-law index of CR energy spectrum as well as the velocity of solar system, and does not vary with energy. The diffusion of CRs also predicts a large-scale dipole anisotropy, whose amplitude is expected to be proportional to the diffusion coefficient and the phase is along the density gradient of CRs. However the observations show a more complicated energy dependence. Less than 100 TeV, the amplitude of anisotropy increases first with energy and then decreases, and is far below the prediction of the standard diffusion scenario [45–48]. Furthermore, the phase also disagrees with the observations. The conventional propagation model predicts the excess of CR flux toward the direction of the Galactic center. However, the TeV measurements show the excess approaches to the direction of the heliotail, i.e. so-called tail-in region [49]. The puzzle is commonly referred to as the “anisotropy problem”. The anisotropy problem may indicate the effects due to the regulation of local magnetic field and/or nearby sources [50–55].

It has been noted that there exists a common energy scale between the structures of the energy spectra and the large-scale anisotropies, which may indicate a common origin of them [56]. We proposed in a recent work that these features might be the imprints of local sources [56]. The spectral softenings around 10 TeV are due to a nearby source contribution on top of the background component. The low-energy ($\lesssim 100$ TeV) anisotropies are dominated by the local source, while the high-energy anisotropies are due to the background. The transition of the low-energy and high-energy components occur at about 100 TeV, forming a dip in the amplitude and a flip of the phase from nearly anti-Galactic center direction to the Galactic center direction. In [56], only protons and Helium nuclei are considered. In this work, we further extend this model to heavier nuclei. We pay particular attention to the anisotropy features of different mass composition (or mass groups), which may be tested in the near future by e.g., LHAASO [57, 58].

2 Model Description

2.1 Spatially-dependent diffusion

We work in a spatially-dependent propagation (SDP) frame, which is motivated by the HAWC observations of extended haloes around pulsars [59]. The SDP model was proposed to account for the hundred GeV spectral hardenings of CRs [21, 60, 61]. It was then found to be able to explain a series of observations of CR spectra and diffuse γ -rays [62, 63]. The diffusion volume in the SDP model is separated into two regions. Close to the Galactic disk ($|z| < \xi z_h$), where z_h is the half thickness of the whole diffusive halo, the level of turbulence is expected to be high due to activities of supernova explosions, and hence the diffusion coefficient is relatively small. In the outer halo ($|z| > \xi z_h$), particles diffuse much faster. The parameterized diffusion coefficient we adopt is [62, 63]

$$D_{xx}(r, z, \mathcal{R}) = D_0 F(r, z) \beta^\eta \left(\frac{\mathcal{R}}{\mathcal{R}_0} \right)^{\delta_0 F(r, z)}, \quad (2.1)$$

where

$$F(r, z) = \begin{cases} g(r, z) + [1 - g(r, z)] \left(\frac{z}{\xi z_0} \right)^n, & |z| \leq \xi z_0, \\ 1, & |z| > \xi z_0 \end{cases}, \quad (2.2)$$

with $g(r, z) = N_m/[1 + f(r, z)]$, and $f(r, z)$ is the source density distribution. The numerical package DRAGON [64] is used to solve the transport equation. In this work, we adopt the diffusion-reacceleration model.

The injection spectrum of background sources is assumed to be a power-law of rigidity with a high-energy exponential cutoff, $q(\mathcal{R}) \propto \mathcal{R}^{-\nu} \exp(-\mathcal{R}/\mathcal{R}_c)$. The cutoff rigidity of each element could be either Z - or A -dependent. The spatial distribution of sources takes the form of SNR distribution [65], $f(r, z) \propto (r/r_\odot)^{1.69} \exp[-3.33(r - r_\odot)/r_\odot] \exp(-|z|/z_s)$, where $r_\odot = 8.5$ kpc and $z_s = 0.2$ kpc.

2.2 Local source

The time-dependent propagation of CRs from the local source is obtained using the Green's function method, assuming a spherical geometry with infinite boundary conditions. The solution is

$$\phi(r, \mathcal{R}, t) = \frac{q_{\text{inj}}(\mathcal{R})}{(\sqrt{2\pi}\sigma)^3} \exp\left(-\frac{r^2}{2\sigma^2}\right), \quad (2.3)$$

where $q_{\text{inj}}(\mathcal{R})\delta(t)\delta(\vec{r})$ is the instantaneous injection spectrum of a point source, $\sigma(\mathcal{R}, t) = \sqrt{2D(\mathcal{R})t}$ is the effective diffusion length within time t . The diffusion coefficient $D(\mathcal{R})$ is taken the value nearby the solar system. The injection spectrum is again parameterized as a cutoff power-law form, $q_{\text{inj}}(\mathcal{R}) = q_0 \mathcal{R}^{-\alpha} \exp(-\mathcal{R}/\mathcal{R}'_c)$. The normalization q_0 is determined through fitting to the GCR energy spectra. The distance and age of the local source are set to be $d = 330$ pc and $\tau = 3.2 \times 10^5$ years [56], respectively. The direction of the local source is obtained through fitting to the data of the anisotropies. We find that for $l = 161^\circ$ and $b = 9^\circ$, both the amplitudes and phases of the large-scale anisotropies can be reproduced (see below). We further assume that the local source contributes only to primary nuclei (such as p, He, C, O, Fe), rather than secondary nuclei (such as B and Be).

2.3 Sun's vertical location

It should be noted that usually the solar system is assumed to be located at the mid-plane of the Galactic disk, and the source distribution is symmetric above and below the disk. However, it has long been known that the Sun locates slightly above the Galactic plane (towards the north Galactic pole). The inferred distance above the mid-plane is from several parsecs to ~ 20 pc [66–68]. The offset may induce a net vertical flow outwards from the Galactic plane, which generates a corresponding component of anisotropy. The total large-scale anisotropies thus include three components, the radial component, the vertical component, and the local source component. The sum of these three components give the total anisotropies which can be used to compare with the data. The vertical location of the Sun is assumed to be 10 pc above the Galactic mid-plane in this work.

3 Results

The model parameters are tuned according to the B/C and $^{10}\text{Be}/^9\text{Be}$ ratios, the energy spectra of various nuclei species, the all-particle spectra, and the amplitudes and phases of

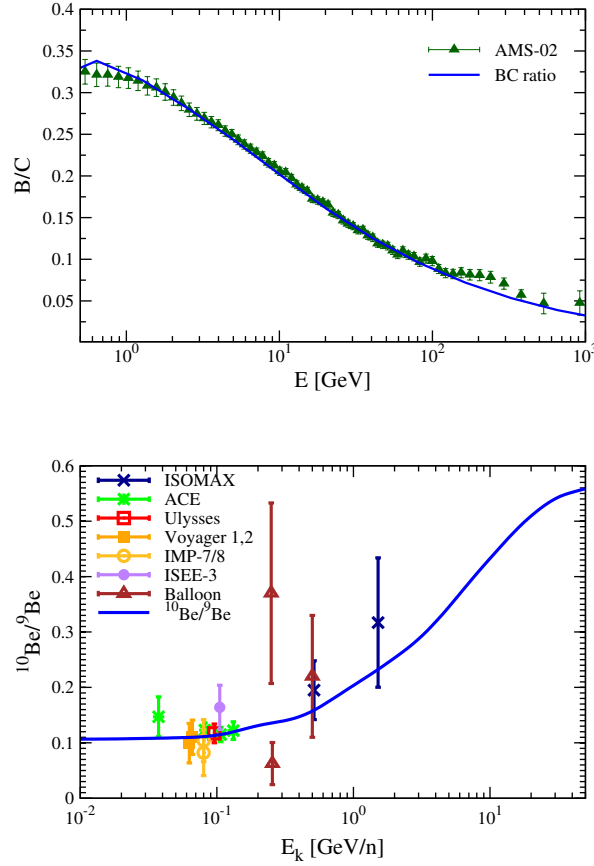


Figure 1. Model predictions of the B/C ratio (left panel) and $^{10}\text{Be}/^9\text{Be}$ ratio (right panel), compared with the measurements [71].

the anisotropies. The diffusion coefficient parameters are $D_0 = 8.34 \times 10^{28} \text{ cm}^2 \text{ s}^{-1}$, $\delta_0 = 0.65$, $N_m = 0.39$, $n = 3.5$, $\xi = 0.1$, and $\eta = 0.05$. The thickness of the propagation halo is $z_h = 10$ kpc, and the Alfvénic velocity is $v_A = 6 \text{ km s}^{-1}$. Note that a larger value of z_h is adopted in this work compared with Ref. [62]. This is to suppress the vertical component of the anisotropies which seems to be lack in the observations at high energies ($> 100 \text{ TeV}$). It is interesting to note that previous studies under the simple one-zone propagation framework also give a relatively large value of the halo height [69, 70]. The comparison of the B/C and $^{10}\text{Be}/^9\text{Be}$ ratios between the model predictions and the data is given in Fig. 1.

Fig. 2 shows the propagated spectra of primary CR components, including protons, He, C, N, O, Ne, Mg, Si, and Fe nuclei. In each panel the blue and red lines are the contributions from the background and the local source respectively, and the black solid line is the sum of them. The corresponding injection parameters are given in Table 1. The spectral indices of the local source component are assumed to be slightly harder than that of the background component, which helps fit the data better. This is reasonable due to the diversity of CR sources, as can be inferred from the γ -ray observations of SNRs [87]. We can see that the addition of the local source component can simultaneously account for the spectral hardening features at $\sim 200 \text{ GV}$, and the softening features at $\sim 10 \text{ TV}$. The SDP model can also give a concave shape of the propagated CR spectra, which was previously proposed to account for

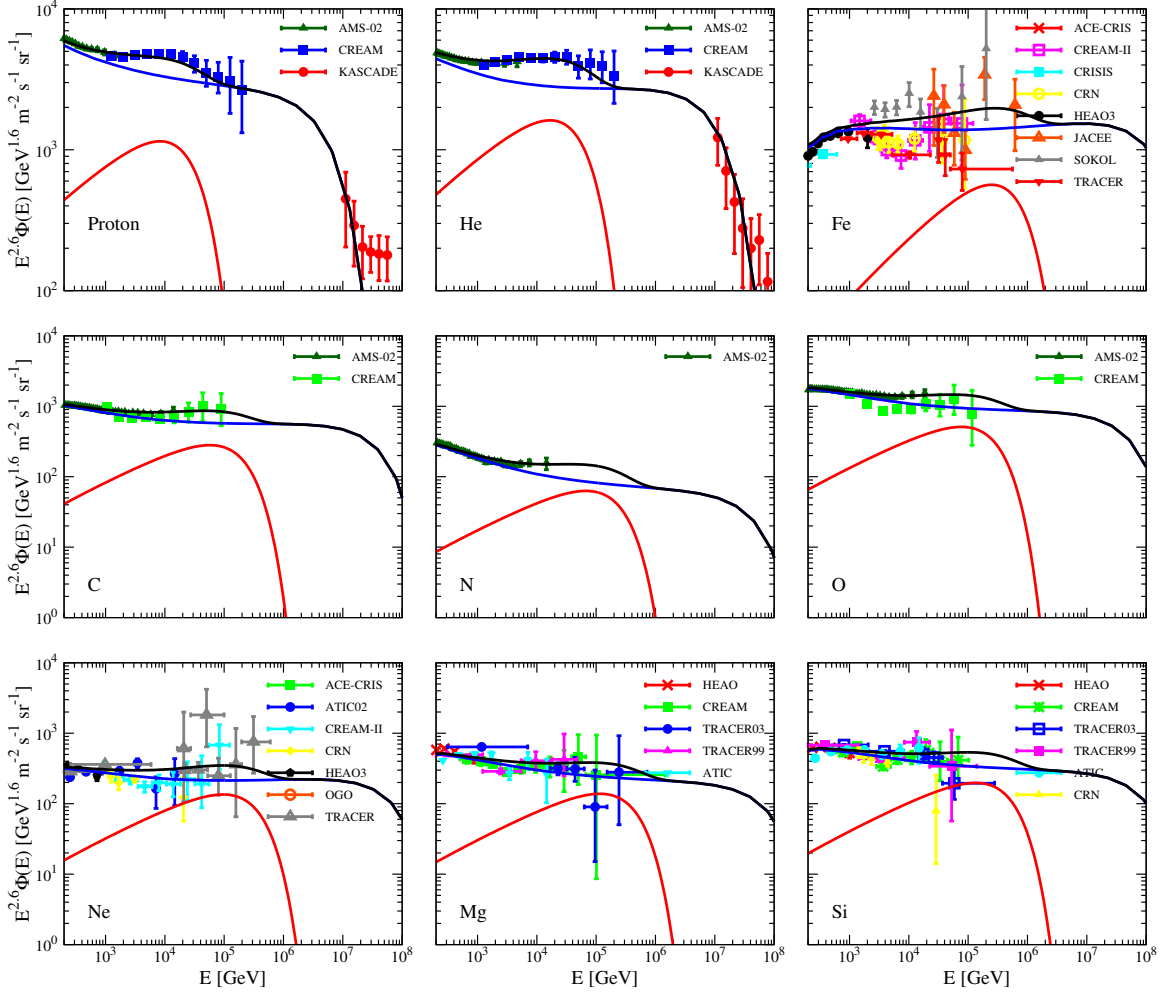


Figure 2. The computed energy spectra of protons, He, C, N, O, Ne, Mg, Si, and Fe nuclei. Here the flux is multiplied by $E^{2.6}$. The red and blue lines are the fluxes from the local and background sources, and the black line is their sum. For protons, He, C, N and O, the data points are taken from AMS-02 [13, 72–74], CREAM [23, 75], and KASCADE [76], respectively. For Ne, Mg, Si, and Fe, the data points are from HEAO [77], TRACER [78–80], ATIC [9], JACEE [81, 82], SOKOL [83], CRISIS [84], ACE-CRIS [85], CRN [86].

the spectral hardenings [62, 63]. However, in this work the SDP-induced spectral hardenings do not specifically correspond to the measured hardenings. Nevertheless, the SDP model is still necessary in suppressing the anisotropies as will be shown below.

Through adding different compositions together, we get the all-particle spectrum as shown in Fig. 3, compared with the weighted data [88]. The knee structure of the all-particle spectrum can be properly reproduced by the background component assuming a Z -dependent cutoff with $\mathcal{R}_c \sim 7$ PV. In this case we find that the knee of the all-particle spectrum is mainly due to the suppression of the light components (protons and He nuclei). This is because we try to fit the KASCADE spectra of protons and He [76]. If alternatively the light component spectra from the Tibet experiments [89] are used, a smaller cutoff rigidity would be obtained

	Background			Local source		
Element	Normalization [†]	ν	\mathcal{R}_c	q_0	α	\mathcal{R}'_c
	$[(\text{m}^2 \cdot \text{sr} \cdot \text{s} \cdot \text{GeV})^{-1}]$		[PV]	$[\text{GeV}^{-1}]$		[TV]
p	8.04×10^{-5}	2.45	7	2.72×10^{52}	2.10	28
He	5.47×10^{-5}	2.39	7	2.53×10^{52}	2.10	28
C	1.12×10^{-5}	2.40	7	4.80×10^{50}	2.05	28
N	1.45×10^{-6}	2.45	7	8.40×10^{49}	2.05	28
O	2.30×10^{-5}	2.43	7	5.50×10^{50}	2.05	28
Ne	4.46×10^{-6}	2.38	7	1.02×10^{50}	2.05	28
Mg	9.06×10^{-6}	2.44	7	7.80×10^{49}	2.05	28
Si	1.03×10^{-5}	2.44	7	8.70×10^{49}	2.05	28
Fe	2.53×10^{-5}	2.38	7	1.01×10^{50}	2.05	28

[†]The normalization is set at total energy $E = 1$ TeV.

Table 1. Injection parameters of the background and local source.

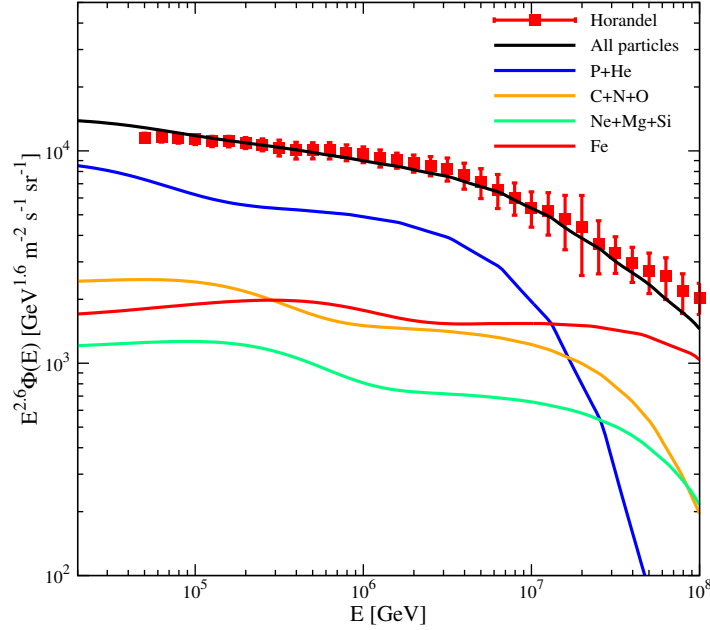


Figure 3. Model prediction of the all-particle spectra, compared with the weighted data [88].

[90].

As suggested in Ref. [56], the softening features in the energy spectra and the energy-dependent anisotropies might have a common origin. In Ref. [56], only the light components of protons and Helium nuclei were considered. Here we add all the major compositions as shown in Fig. 2 together. The corresponding amplitudes and phases of the dipole anisotropies are given in Fig. 4. The energy dependences of both the amplitudes and phases can be well reproduced in this model. Compared with Ref. [56], the dip of the amplitudes becomes wider, which matches better with the data. The transition of the phase also becomes smoother, and

can be tested by improved measurements in future. Note that the direction of the local source is different from that assumed in Ref. [56], due to the inclusion of the vertical anisotropies in this work.

We further calculate the anisotropies of different compositions. Considering the limited particle identification capability of the ground-based experiments, the primary components are divided into four mass groups, i.e. $p+\text{He}$, $\text{C}+\text{N}+\text{O}$, $\text{Ne}+\text{Mg}+\text{Si}$, and Fe , respectively. The resulting anisotropies are shown in Fig. 5. Dip structures of the amplitudes and phase flippings are visible for each mass group. We expect that the observations of anisotropies of different mass groups by LHAASO would be promising in revealing these structures, and give a critical test of this model.

The above discussion is based on the assumption of a Z -dependent cutoff energy of the local source spectra. We further investigate the effect due to an A -dependent cutoff. The comparison of the anisotropy amplitudes and phases of protons and Helium nuclei for Z - and A -dependent cutoff are shown in Fig. 6. For both cases, the model parameters are tuned to fit the energy spectra of different compositions and the total anisotropies. It is clearly shown that the energies of the dip of protons and Helium nuclei can effectively distinguish these two assumptions. A clear identification of protons and Helium individually is a little bit challenging for ground-based experiments [91]. The measurements of anisotropies of protons and $p+\text{He}$ are possible for the LHAASO experiment [91], which can also be very important in probing the Z - and A -dependent cutoff assumptions of the model.

4 Discussion

Measurements of CRs enter a precise era thanks to fast development of space and ground-based experiments in recent years. Based on the new features of the CR spectra, including the spectral hardenings at ~ 200 GV and softenings at ~ 10 TV, together with the inhomogeneous diffusion inferred by the HAWC observations of pulsars and the long time puzzle of the energy-dependent evolution of the dipole anisotropy features, an SDP frame with contributions from a local CR source was established and could explain most of these new observational facts [56].

In this work, we extend this model to study the anisotropies of heavier nuclei. We find that the dip structure (phase flipping) of the total amplitudes (phases) of the anisotropies becomes smoother after adding heavier nuclei. This is because the dip features and phase changes for different species depend on energy, and the measurements of all species of CRs give an average effect of them. The anisotropies of different mass groups are also investigated. Similar dip features and phase changes are predicted for all of these compositions, with different characteristic energies. We further explore the differences of the large-scale anisotropy features between Z - and A -dependent assumptions of cutoff of the local source spectra. It is expected that future precise measurements of the anisotropies of different compositions or mass groups by e.g., DAMPE [113], HERD [114], and LHAASO [58].

Finally we comment that the spectral features of the electrons and positrons, particularly the remarkable positron excess (e.g., [115, 116]), can also be properly reproduced under the same framework of the source and propagation models as discussed in this work [117]. It is thus very encouraging to establish a unified scenario of GCR origin and propagation based on new precise observations of CRs and γ -rays.

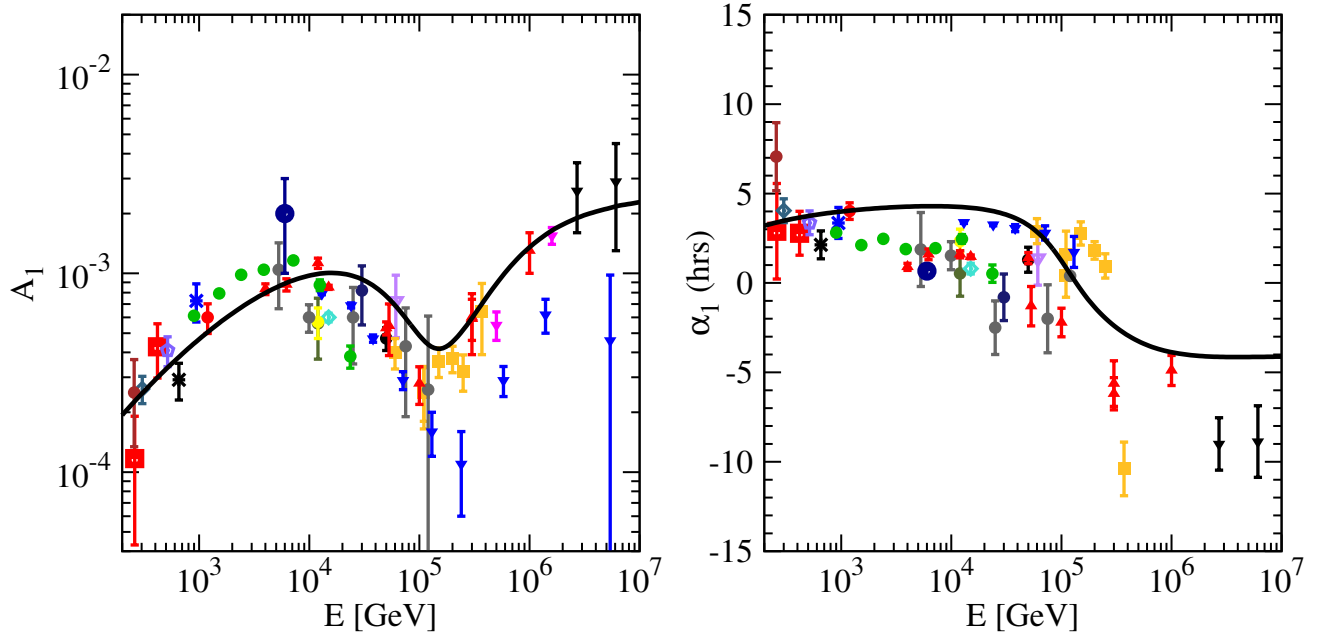


Figure 4. The energy dependence of the amplitudes (left) and phases (right) of the dipole anisotropies when adding all of the major elements together. The data points are taken from underground muon detectors: Norikura (1973; [92]), Ottawa (1983; [93]), London (1983; [94]), Bolivia (1985; [95]), Budapest (1985; [95]), Hobart (1985; [95]), London (1985; [95]), Misato (1985; [95]), Socorro (1985; [95]), Yakutsk (1985; [95]), Banksan (1987; [96]), Hong Kong (1987; [97]), Sakashita (1990; [98]), Utah (1991; [99]), Liapootah (1995; [100]), Matsushiro (1995; [101]), Poatina (1995; [102]), Kamiokande (1997; [103]), Marco (2003; [104]), SuperKamiokande (2007; [27]); and air shower array experiments: PeakMusala (1975; [105]), Baksan (1981; [106]), Norikura (1989; [107]), EAS-TOP (1995, 1996, 2009; [108–110]), Baksan (2009; [111]), Milagro (2009; [33]), IceCube (2010, 2012; [34, 36]), Ice-Top (2013; [37]), ARGO-YBJ (2015; [40]), Tibet (2005, 2015, 2017; [28, 31, 112]).

Acknowledgments

This work is supported by the National Key Research and Development Program of China (No. 2018YFA0404203), the National Natural Science Foundation of China (Nos. 11875264, 11635011, 11761141001, 11663006, 11722328, 11851305).

References

- [1] W. I. Axford, E. Leer, and G. Skadron. The acceleration of cosmic rays by shock waves. In *International Cosmic Ray Conference*, volume 11 of *International Cosmic Ray Conference*, pages 132–137, 1977.
- [2] G. F. Krymskii. A regular mechanism for the acceleration of charged particles on the front of a shock wave. *Akademiia Nauk SSSR Doklady*, 234:1306–1308, June 1977.
- [3] A. R. Bell. The acceleration of cosmic rays in shock fronts. I. *Mon. Not. Roy. Astron. Soc.*, 182:147–156, January 1978.

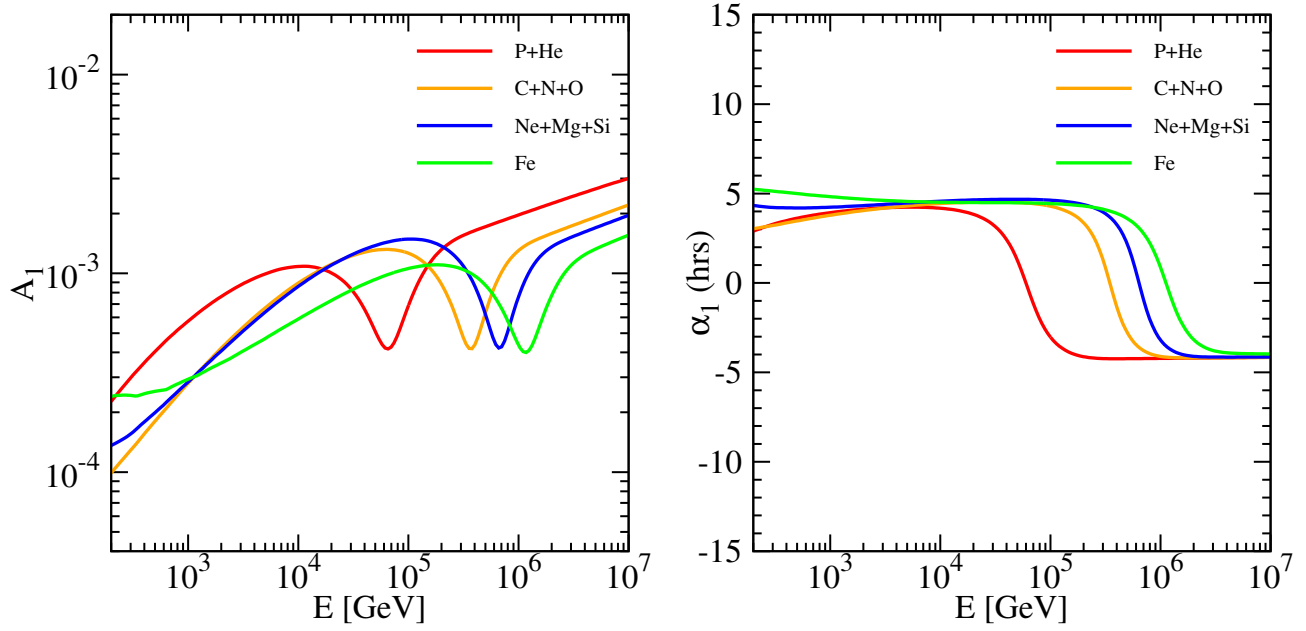


Figure 5. The energy dependence of amplitudes and phases of the dipole anisotropies for four mass groups, p+He, C+N+O, Ne+Mg+Si, and Fe, respectively.

- [4] R. D. Blandford and J. P. Ostriker. Particle acceleration by astrophysical shocks. *Astrophys. J. Lett.* , 221:L29–L32, April 1978.
- [5] Q. Yuan, S.-J. Lin, K. Fang, and X.-J. Bi. Propagation of cosmic rays in the AMS-02 era. *Phys. Rev. D* , 95(8):083007, April 2017.
- [6] V. S. Berezhinskii, S. V. Bulanov, V. A. Dogiel, and V. S. Ptuskin. *Astrophysics of cosmic rays*. Amsterdam: North-Holland, 1990, edited by Ginzburg, V.L., 1990.
- [7] A. W. Strong, I. V. Moskalenko, and V. S. Ptuskin. Cosmic-Ray Propagation and Interactions in the Galaxy. *Annual Review of Nuclear and Particle Science*, 57:285–327, November 2007.
- [8] A. D. Panov, J. H. Adams, Jr., H. S. Ahn, et al. Elemental energy spectra of cosmic rays from the data of the ATIC-2 experiment. *Bull. Russ. Acad. Sci. Phys.*, 71:494–497, April 2007.
- [9] A. D. Panov, J. H. Adams, H. S. Ahn, et al. Energy spectra of abundant nuclei of primary cosmic rays from the data of ATIC-2 experiment: Final results. *Bulletin of the Russian Academy of Sciences, Physics*, 73:564–567, June 2009.
- [10] H. S. Ahn, P. Allison, M. G. Bagliesi, et al. Discrepant Hardening Observed in Cosmic-ray Elemental Spectra. *Astrophys. J. Lett.* , 714:L89–L93, May 2010.
- [11] Y. S. Yoon, H. S. Ahn, P. S. Allison, et al. Cosmic-ray Proton and Helium Spectra from the First CREAM Flight. *Astrophys. J.* , 728:122, February 2011.
- [12] O. Adriani, G. C. Barbarino, G. A. Bazilevskaya, et al. PAMELA Measurements of Cosmic-Ray Proton and Helium Spectra. *Science*, 332:69–, April 2011.
- [13] M. Aguilar, D. Aisa, B. Alpat, et al. Precision Measurement of the Proton Flux in Primary

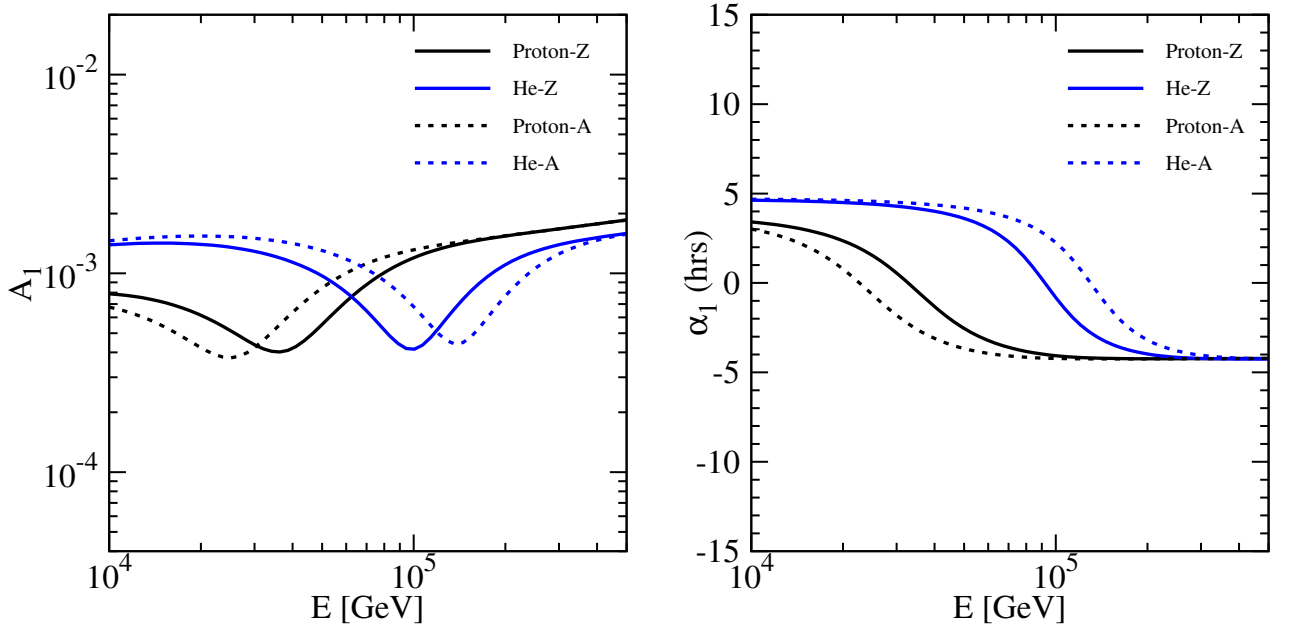


Figure 6. Comparison of the amplitudes (left) and phases (right) of the anisotropies of protons and Helium between Z- and A-dependent cutoff of the local source spectra.

Cosmic Rays from Rigidity 1 GV to 1.8 TV with the Alpha Magnetic Spectrometer on the International Space Station. *Physical Review Letters*, 114(17):171103, May 2015.

- [14] M. Aguilar, D. Aisa, B. Alpat, et al. Precision Measurement of the Helium Flux in Primary Cosmic Rays of Rigidities 1.9 GV to 3 TV with the Alpha Magnetic Spectrometer on the International Space Station. *Physical Review Letters*, 115(21):211101, November 2015.
- [15] O. Adriani, Y. Akaike, K. Asano, et al. Direct Measurement of the Cosmic-Ray Proton Spectrum from 50 GeV to 10 TeV with the Calorimetric Electron Telescope on the International Space Station. *Phys. Rev. Lett.* , 122(18):181102, May 2019.
- [16] Y. Ohira and K. Ioka. Cosmic-ray Helium Hardening. *Astrophys. J. Lett.* , 729:L13, March 2011.
- [17] M. A. Malkov, P. H. Diamond, and R. Z. Sagdeev. Proton-Helium Spectral Anomaly as a Signature of Cosmic Ray Accelerator. *Physical Review Letters*, 108(8):081104, February 2012.
- [18] Q. Yuan, B. Zhang, and X.-J. Bi. Cosmic ray spectral hardening due to dispersion in the source injection spectra. *Phys. Rev. D* , 84(4):043002, August 2011.
- [19] P. Blasi, E. Amato, and P. D. Serpico. Spectral Breaks as a Signature of Cosmic Ray Induced Turbulence in the Galaxy. *Physical Review Letters*, 109(6):061101, August 2012.
- [20] A. E. Vladimirov, G. Jóhannesson, I. V. Moskalenko, and T. A. Porter. Testing the Origin of High-energy Cosmic Rays. *Astrophys. J.* , 752:68, June 2012.
- [21] N. Tomassetti. Origin of the Cosmic-Ray Spectral Hardening. *Astrophys. J. Lett.* , 752:L13, June 2012.
- [22] Q. An, R. Asfandiyarov, P. Azzarello, et al. Measurement of the cosmic-ray proton spectrum

from 40 GeV to 100 TeV with the DAMPE satellite. *Science Advances*, 5(9):eaax3793, Sep 2019.

- [23] Y. S. Yoon, T. Anderson, A. Barrau, et al. Proton and Helium Spectra from the CREAM-III Flight. *Astrophys. J.* , 839:5, April 2017.
- [24] E. Atkin, V. Bulatov, V. Dorokhov, et al. New Universal Cosmic-Ray Knee near a Magnetic Rigidity of 10 TV with the NUCLEON Space Observatory. *Soviet Journal of Experimental and Theoretical Physics Letters*, 108:5–12, July 2018.
- [25] Chuan Yue, Peng-Xiong Ma, Qiang Yuan, et al. Implications on the origin of cosmic rays in light of 10 TV spectral softenings. *arXiv e-prints*, page arXiv:1909.12857, Sep 2019.
- [26] Paolo Lipari and Silvia Vernetto. The shape of the cosmic ray proton spectrum. *arXiv e-prints*, page arXiv:1911.01311, Nov 2019.
- [27] G. Guillian, J. Hosaka, K. Ishihara, et al. Observation of the anisotropy of 10TeV primary cosmic ray nuclei flux with the Super-Kamiokande-I detector. *Phys. Rev. D* , 75(6):062003, March 2007.
- [28] M. Amenomori, S. Ayabe, S. W. Cui, et al. Large-Scale Sidereal Anisotropy of Galactic Cosmic-Ray Intensity Observed by the Tibet Air Shower Array. *Astrophys. J. Lett.* , 626:L29–L32, June 2005.
- [29] M. Amenomori, S. Ayabe, X. J. Bi, et al. Anisotropy and Corotation of Galactic Cosmic Rays. *Science*, 314:439–443, October 2006.
- [30] M. Amenomori, X. J. Bi, D. Chen, et al. On Temporal Variations of the Multi-TeV Cosmic Ray Anisotropy Using the Tibet III Air Shower Array. *Astrophys. J.* , 711:119–124, March 2010.
- [31] M. Amenomori, X. J. Bi, D. Chen, et al. Northern Sky Galactic Cosmic Ray Anisotropy between 10 and 1000 TeV with the Tibet Air Shower Array. *Astrophys. J.* , 836:153, February 2017.
- [32] A. A. Abdo, B. Allen, T. Aune, et al. Discovery of Localized Regions of Excess 10-TeV Cosmic Rays. *Physical Review Letters*, 101(22):221101, November 2008.
- [33] A. A. Abdo, B. T. Allen, T. Aune, et al. The Large-Scale Cosmic-Ray Anisotropy as Observed with Milagro. *Astrophys. J.* , 698:2121–2130, June 2009.
- [34] R. Abbasi, Y. Abdou, T. Abu-Zayyad, et al. Measurement of the Anisotropy of Cosmic-ray Arrival Directions with IceCube. *Astrophys. J. Lett.* , 718:L194–L198, August 2010.
- [35] R. Abbasi, Y. Abdou, T. Abu-Zayyad, et al. Observation of Anisotropy in the Arrival Directions of Galactic Cosmic Rays at Multiple Angular Scales with IceCube. *Astrophys. J.* , 740:16, October 2011.
- [36] R. Abbasi, Y. Abdou, T. Abu-Zayyad, et al. Observation of Anisotropy in the Galactic Cosmic-Ray Arrival Directions at 400 TeV with IceCube. *Astrophys. J.* , 746:33, February 2012.
- [37] M. G. Aartsen, R. Abbasi, Y. Abdou, et al. Observation of Cosmic-Ray Anisotropy with the IceTop Air Shower Array. *Astrophys. J.* , 765:55, March 2013.
- [38] M. G. Aartsen, K. Abraham, M. Ackermann, et al. Anisotropy in Cosmic-Ray Arrival Directions in the Southern Hemisphere Based on Six Years of Data from the IceCube Detector. *Astrophys. J.* , 826:220, August 2016.
- [39] B. Bartoli, P. Bernardini, X. J. Bi, et al. Medium scale anisotropy in the TeV cosmic ray flux observed by ARGO-YBJ. *Phys. Rev. D* , 88(8):082001, October 2013.

- [40] B. Bartoli, P. Bernardini, X. J. Bi, et al. ARGO-YBJ Observation of the Large-scale Cosmic Ray Anisotropy During the Solar Minimum between Cycles 23 and 24. *Astrophys. J.* , 809:90, August 2015.
- [41] A. U. Abeysekara, R. Alfaro, C. Alvarez, et al. Observation of Small-scale Anisotropy in the Arrival Direction Distribution of TeV Cosmic Rays with HAWC. *Astrophys. J.* , 796:108, December 2014.
- [42] A. U. Abeysekara, R. Alfaro, C. Alvarez, et al. All-sky Measurement of the Anisotropy of Cosmic Rays at 10 TeV and Mapping of the Local Interstellar Magnetic Field. *Astrophys. J.* , 871:96, January 2019.
- [43] A. H. Compton and I. A. Getting. An Apparent Effect of Galactic Rotation on the Intensity of Cosmic Rays. *Physical Review*, 47:817–821, June 1935.
- [44] L. J. Gleeson and W. I. Axford. The Compton-Getting Effect. *Astrophys. Space Sci.* , 2:431–437, December 1968.
- [45] A. M. Hillas. TOPICAL REVIEW: Can diffusive shock acceleration in supernova remnants account for high-energy galactic cosmic rays? *Journal of Physics G Nuclear Physics*, 31:R95–R131, May 2005.
- [46] A. D. Erlykin and A. W. Wolfendale. The anisotropy of galactic cosmic rays as a product of stochastic supernova explosions. *Astroparticle Physics*, 25:183–194, April 2006.
- [47] V. S. Ptuskin, F. C. Jones, E. S. Seo, and R. Sina. Effect of random nature of cosmic ray sources Supernova remnants on cosmic ray intensity fluctuations, anisotropy, and electron energy spectrum. *Advances in Space Research*, 37:1909–1912, 2006.
- [48] P. Blasi and E. Amato. Diffusive propagation of cosmic rays from supernova remnants in the Galaxy. II: anisotropy. *JCAP*, 1:11, January 2012.
- [49] K. Nagashima, K. Fujimoto, and R. M. Jacklyn. Galactic and heliotail-in anisotropies of cosmic rays as the origin of sidereal daily variation in the energy region $< 10^4 \text{ GeV}$. *J. Geophys. Res.*, 103:17429–17440, August 1998.
- [50] N. A. Schwadron, F. C. Adams, E. R. Christian, et al. Global Anisotropies in TeV Cosmic Rays Related to the Sun’s Local Galactic Environment from IBEX. *Science*, 343:988–990, February 2014.
- [51] V. Savchenko, M. Kachelrieß, and D. V. Semikoz. Imprint of a 2 Million Year Old Source on the Cosmic-Ray Anisotropy. *Astrophys. J. Lett.* , 809:L23, August 2015.
- [52] P. Mertsch and S. Funk. Solution to the Cosmic Ray Anisotropy Problem. *Physical Review Letters*, 114(2):021101, January 2015.
- [53] M. Ahlers. Deciphering the Dipole Anisotropy of Galactic Cosmic Rays. *Physical Review Letters*, 117(15):151103, October 2016.
- [54] L. G. Sveshnikova, O. N. Strelnikova, and V. S. Ptuskin. Spectrum and anisotropy of cosmic rays at TeV-PeV-energies and contribution of nearby sources. *Astroparticle Physics*, 50:33–46, December 2013.
- [55] W. Liu, X.-J. Bi, S.-J. Lin, B.-B. Wang, and P.-F. Yin. Excesses of cosmic ray spectra from a single nearby source. *Phys. Rev. D* , 96(2):023006, July 2017.
- [56] Wei Liu, Yi-Qing Guo, and Qiang Yuan. Indication of nearby source signatures of cosmic rays from energy spectra and anisotropies. *JCAP*, 2019(10):010, Oct 2019.
- [57] Z. Cao. A future project at tibet: the large high altitude air shower observatory (LHAASO). *Chinese Physics C*, 34:249–252, February 2010.
- [58] X. Bai, B. Y. Bi, X. J. Bi, et al. The Large High Altitude Air Shower Observatory (LHAASO) Science White Paper. *arXiv e-prints*, May 2019.

- [59] A. U. Abeysekara, A. Albert, R. Alfaro, et al. Extended gamma-ray sources around pulsars constrain the origin of the positron flux at Earth. *Science*, 358:911–914, November 2017.
- [60] Y.-Q. Guo, Z. Tian, and C. Jin. Spatial-dependent Propagation of Cosmic Rays Results in the Spectrum of Proton, Ratios of P/P, and B/C, and Anisotropy of Nuclei. *Astrophys. J.* , 819:54, March 2016.
- [61] C. Jin, Y.-Q. Guo, and H.-B. Hu. Spatial dependent diffusion of cosmic rays and the excess of primary electrons derived from high precision measurements by AMS-02. *Chinese Physics C*, 40(1):015101, January 2016.
- [62] Y.-Q. Guo and Q. Yuan. Understanding the spectral hardenings and radial distribution of Galactic cosmic rays and Fermi diffuse γ rays with spatially-dependent propagation. *Phys. Rev. D* , 97(6):063008, March 2018.
- [63] W. Liu, Y.-h. Yao, and Y.-Q. Guo. Revisiting the Spatially Dependent Propagation Model with the Latest Observations of Cosmic-Ray Nuclei. *Astrophys. J.* , 869:176, December 2018.
- [64] C. Evoli, D. Gaggero, D. Grasso, and L. Maccione. Cosmic ray nuclei, antiprotons and gamma rays in the galaxy: a new diffusion model. *JCAP*, 10:018, October 2008.
- [65] G. Case and D. Bhattacharya. Revisiting the galactic supernova remnant distribution. *A&AS*, 120:437–440, December 1996.
- [66] Y. C. Joshi. Displacement of the Sun from the Galactic plane. *Mon. Not. Roy. Astron. Soc.* , 378(2):768–776, Jun 2007.
- [67] V. V. Bobylev and A. T. Bajkova. The z distribution of hydrogen clouds and masers with kinematic distances. *Astronomy Letters*, 42(3):182–192, Mar 2016.
- [68] J. M. Yao, R. N. Manchester, and N. Wang. Determination of the Sun’s offset from the Galactic plane using pulsars. *Mon. Not. Roy. Astron. Soc.* , 468(3):3289–3294, Jul 2017.
- [69] M. Ackermann, M. Ajello, L. Baldini, et al. Constraints on the Cosmic-ray Density Gradient Beyond the Solar Circle from Fermi γ -ray Observations of the Third Galactic Quadrant. *Astrophys. J.* , 726:81, January 2011.
- [70] Elena Orlando and Andrew Strong. Galactic synchrotron emission with cosmic ray propagation models. *Mon. Not. Roy. Astron. Soc.* , 436(3):2127–2142, Dec 2013.
- [71] Su-Jie Lin, Qiang Yuan, and Xiao-Jun Bi. Quantitative study of the ams-02 electron/positron spectra: Implications for pulsars and dark matter properties. *Phys. Rev. D*, 91:063508, Mar 2015.
- [72] M. Aguilar, L. Ali Cavazonza, B. Alpat, et al. Observation of the Identical Rigidity Dependence of He, C, and O Cosmic Rays at High Rigidities by the Alpha Magnetic Spectrometer on the International Space Station. *Physical Review Letters*, 119(25):251101, December 2017.
- [73] M. Aguilar, L. Ali Cavazonza, G. Ambrosi, et al. Observation of New Properties of Secondary Cosmic Rays Lithium, Beryllium, and Boron by the Alpha Magnetic Spectrometer on the International Space Station. *Physical Review Letters*, 120(2):021101, January 2018.
- [74] M. Aguilar, L. Ali Cavazonza, B. Alpat, et al. Precision Measurement of Cosmic-Ray Nitrogen and its Primary and Secondary Components with the Alpha Magnetic Spectrometer on the International Space Station. *Physical Review Letters*, 121(5):051103, August 2018.
- [75] H. S. Ahn, P. Allison, M. G. Bagliesi, et al. Energy Spectra of Cosmic-ray Nuclei at High Energies. *Astrophys. J.* , 707:593–603, December 2009.
- [76] W. D. Apel, J. C. Arteaga-Velázquez, K. Bekk, et al. KASCADE-Grande measurements of energy spectra for elemental groups of cosmic rays. *Astroparticle Physics*, 47:54–66, July 2013.

- [77] J. J. Engelmann, P. Ferrando, A. Soutoul, et al. Charge composition and energy spectra of cosmic-ray nuclei for elements from Be to Ni - Results from HEAO-3-C2. *Astron. Astrophys.* , 233:96–111, July 1990.
- [78] F. Gahbauer, G. Hermann, J. R. Hörandel, D. Müller, and A. A. Radu. A New Measurement of the Intensities of the Heavy Primary Cosmic-Ray Nuclei around 1 TeV amu^{-1} . *Astrophys. J.* , 607:333–341, May 2004.
- [79] M. Ave, P. J. Boyle, F. Gahbauer, et al. Composition of Primary Cosmic-Ray Nuclei at High Energies. *Astrophys. J.* , 678:262–273, May 2008.
- [80] A. Obermeier, M. Ave, P. Boyle, et al. Energy Spectra of Primary and Secondary Cosmic-Ray Nuclei Measured with TRACER. *Astrophys. J.* , 742:14, November 2011.
- [81] Jörg R. Hörandel. A review of experimental results at the knee. In *Journal of Physics Conference Series*, volume 47 of *Journal of Physics Conference Series*, pages 41–50, Oct 2006.
- [82] K. Asakimori, T. H. Burnett, M. L. Cherry, et al. Cosmic-Ray Proton and Helium Spectra: Results from the JACEE Experiment. *Astrophys. J.* , 502:278–283, July 1998.
- [83] I. P. Ivanenko, V. Y. Shestoporov, L. O. Chikova, et al. Energy Spectra of Cosmic Rays above 2 TeV as Measured by the ‘SOKOL’ Apparatus. *International Cosmic Ray Conference*, 2:17, 1993.
- [84] J. S. Young, P. S. Freier, C. J. Waddington, N. R. Brewster, and R. K. Fickle. The elemental and isotopic composition of cosmic rays - Silicon to nickel. *Astrophys. J.* , 246:1014–1030, June 1981.
- [85] K. A. Lave, M. E. Wiedenbeck, W. R. Binns, et al. Galactic Cosmic-Ray Energy Spectra and Composition during the 2009-2010 Solar Minimum Period. *Astrophys. J.* , 770:117, June 2013.
- [86] D. Mueller, S. P. Swordy, P. Meyer, J. L’Heureux, and J. M. Grunsfeld. Energy spectra and composition of primary cosmic rays. *Astrophys. J.* , 374:356–365, June 1991.
- [87] Q. Yuan, P.-F. Yin, and X.-J. Bi. Neutrino emission of Fermi supernova remnants. *Astroparticle Physics*, 35:33–38, August 2011.
- [88] J. R. Hörandel. On the knee in the energy spectrum of cosmic rays. *Astroparticle Physics*, 19:193–220, May 2003.
- [89] B. Bartoli, P. Bernardini, X. J. Bi, et al. Knee of the cosmic hydrogen and helium spectrum below 1 PeV measured by ARGO-YBJ and a Cherenkov telescope of LHAASO. *Phys. Rev. D* , 92(9):092005, November 2015.
- [90] Y.-Q. Guo and Q. Yuan. On the knee of Galactic cosmic rays in light of sub-TeV spectral hardenings. *Chinese Physics C*, 42(7):075103, June 2018.
- [91] L. Q. Yin, S. S. Zhang, Z. Cao, et al. The expectation of cosmic ray proton and helium energy spectrum below 4 PeV measured by LHAASO. *arXiv e-prints*, page arXiv:1904.09130, Apr 2019.
- [92] S. Sakakibara, H. Ueno, K. Fujimoto, I. Kondo, and K. Nagashima. Sidereal Time Variation of Small Air Showers Observed at Mt. Norikura. *International Cosmic Ray Conference*, 2:1058, 1973.
- [93] M. Bercovitch and S. P. Agrawal. Cosmic ray anisotropies at median primary rigidities between 100 and 1000 GV. *International Cosmic Ray Conference*, 10:246–249, 1981.
- [94] T. Thambyahpillai. The Sidereal Diurnal Variation Measured Underground in London. *International Cosmic Ray Conference*, 3:383, August 1983.
- [95] D. B. Swinson and K. Nagashima. Corrected sidereal anisotropy for underground muons. *Planet. Space Sci.*, 33:1069–1072, September 1985.

- [96] Y. M. Andreyev, A. E. Chudakov, V. A. Kozyarivsky, et al. Cosmic Ray Sidereal Anisotropy Observed by Baksan Underground Muon Telescope. *International Cosmic Ray Conference*, 2:22, 1987.
- [97] Y. W. Lee and L. K. Ng. Observation of Cosmic-Ray Intensity Variation Using AN Underground Telescope. *International Cosmic Ray Conference*, 2:18, 1987.
- [98] H. Ueno, Z. Fujii, and T. Yamada. 11 Years Variations of Sidereal Anisotropy Observed at Sakashita Underground Station. *International Cosmic Ray Conference*, 6:361, 1990.
- [99] D. J. Cutler and D. E. Groom. Mayflower Mine 1500 GV detector - Cosmic-ray anisotropy and search for Cygnus X-3. *Astrophys. J.* , 376:322–334, July 1991.
- [100] K. Munakata, S. Yasue, S. Mori, et al. Two Hemisphere Observations of the North-South Sidereal Asymmetry at ~ 1 TeV. *International Cosmic Ray Conference*, 4:639, 1995.
- [101] S. Mori, S. Yasue, K. Munakata, et al. Observation of Sidereal Anisotropy of Cosmic Rays at ~ 1 TV. *International Cosmic Ray Conference*, 4:648, 1995.
- [102] K. B. Fenton, A. G. Fenton, and J. E. Humble. Sidereal Variations at High Energies - Observations at Poatina. *International Cosmic Ray Conference*, 4:635, 1995.
- [103] K. Munakata, T. Kiuchi, S. Yasue, et al. Large-scale anisotropy of the cosmic-ray muon flux in Kamiokande. *Phys. Rev. D* , 56:23–26, July 1997.
- [104] M. Ambrosio, R. Antolini, A. Baldini, et al. Search for the sidereal and solar diurnal modulations in the total MACRO muon data set. *Phys. Rev. D* , 67(4):042002, February 2003.
- [105] T. Gombosi, J. Kóta, A. J. Somogyi, et al. Galactic cosmic ray anisotropy at $\approx 6 \times 10^{13}$ eV. *International Cosmic Ray Conference*, 2:586–591, August 1975.
- [106] V. V. Alexeyenko, A. E. Chudakov, E. N. Gulieva, and V. G. Sborschikov. Anisotropy of Small EAS (about 10(13) Ev). *International Cosmic Ray Conference*, 2:146, 1981.
- [107] K. Nagashima, K. Fujimoto, S. Sakakibara, et al. Galactic cosmic-ray anisotropy and its modulation in the heliomagnetosphere, inferred from air shower observation at Mt. Norikura. *Nuovo Cimento C Geophysics Space Physics C*, 12:695–749, December 1989.
- [108] M. Aglietta, B. Alessandro, P. Antonioli, et al. Study of the Cosmic Ray Anisotropy at $E_o \sim 100$ TeV from EAS-TOP: 1992-1994. *International Cosmic Ray Conference*, 2:800, 1995.
- [109] M. Aglietta, B. Alessandro, P. Antonioli, et al. A Measurement of the Solar and Sidereal Cosmic-Ray Anisotropy at E_0 approximately 10 14 eV. *Astrophys. J.* , 470:501, October 1996.
- [110] M. Aglietta, V. V. Alekseenko, B. Alessandro, et al. Evolution of the Cosmic-Ray Anisotropy Above 10^{14} eV. *Astrophys. J. Lett.* , 692:L130–L133, February 2009.
- [111] V. V. Alekseenko, A. B. Cherniaev, D. D. Djappuev, et al. 10-100 TeV cosmic ray anisotropy measured at the Baksan EAS “Carpet” array. *Nuclear Physics B Proceedings Supplements*, 196:179–182, December 2009.
- [112] M. Amenomori, X. J. Bi, D. Chen, et al. Northern sky Galactic Cosmic Ray anisotropy between 10-1000 TeV with the Tibet Air Shower Array. In *34th International Cosmic Ray Conference (ICRC2015)*, volume 34 of *International Cosmic Ray Conference*, page 355, July 2015.
- [113] J. Chang, G. Ambrosi, Q. An, et al. The DArk Matter Particle Explorer mission. *Astroparticle Physics*, 95:6–24, October 2017.
- [114] S. N. Zhang, O. Adriani, S. Albergo, et al. The high energy cosmic-radiation detection (HERD) facility onboard China’s Space Station. In *Proc. SPIE*, volume 9144, page 91440X, July 2014.
- [115] O. Adriani, G. C. Barbarino, G. A. Bazilevskaya, et al. An anomalous positron abundance in cosmic rays with energies 1.5-100 GeV. *Nature* , 458:607–609, April 2009.

- [116] M. Aguilar, G. Alberti, B. Alpat, et al. First Result from the Alpha Magnetic Spectrometer on the International Space Station: Precision Measurement of the Positron Fraction in Primary Cosmic Rays of 0.5-350 GeV. *Physical Review Letters*, 110(14):141102, April 2013.
- [117] Zhen Tian, Wei Liu, Bo Yang, et al. Electron and positron spectra in the three dimensional spatial-dependent propagation model. *arXiv e-prints*, page arXiv:1904.10663, Apr 2019.